Supporting Material

Phase diagram of SALR fluids on spherical surfaces

Stefano Franzini, Luciano Reatto and Davide Pini

Oct. 20, 2021

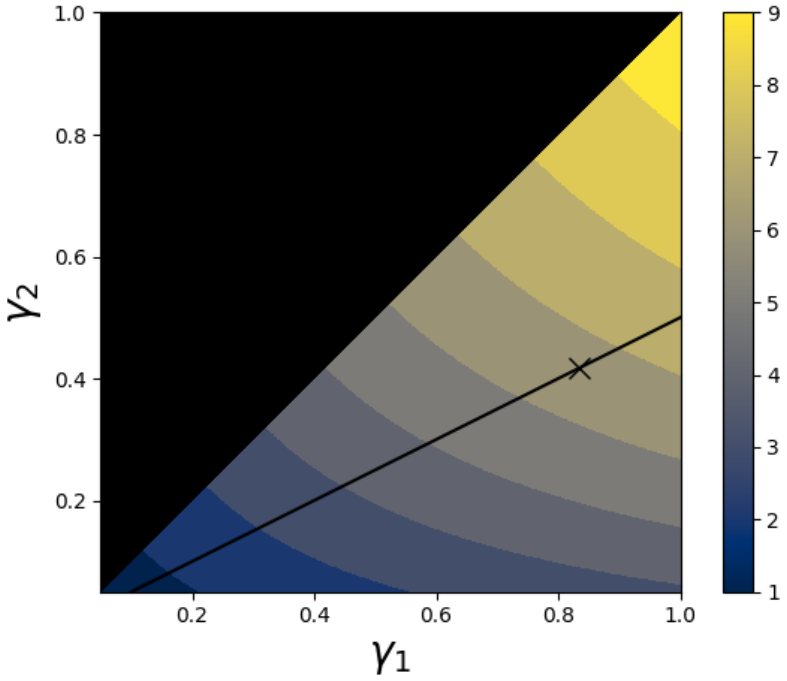

Figure S1: The values taken by ℓ^* as a function of γ_1 and γ_2, at $\sigma/R = 0.1$. The values taken by γ_1 γ_2 are chosen so that the range of the potential is always between the size of the particle (σ^*) and the diameter of the sphere $2R$. The black background corresponds to regions that have not been explored (where $\gamma_1 < \gamma_2$). The solid black line corresponds to $\gamma_1 = 2\gamma_2$, and the cross denotes the choice $\gamma_1 = \frac{5}{6}$ and $\gamma_2 = \frac{1}{2}\gamma_1$.

References

[Driscoll and Healy(1994)] J. Driscoll and D. Healy, 1994, **15**, 202–250.

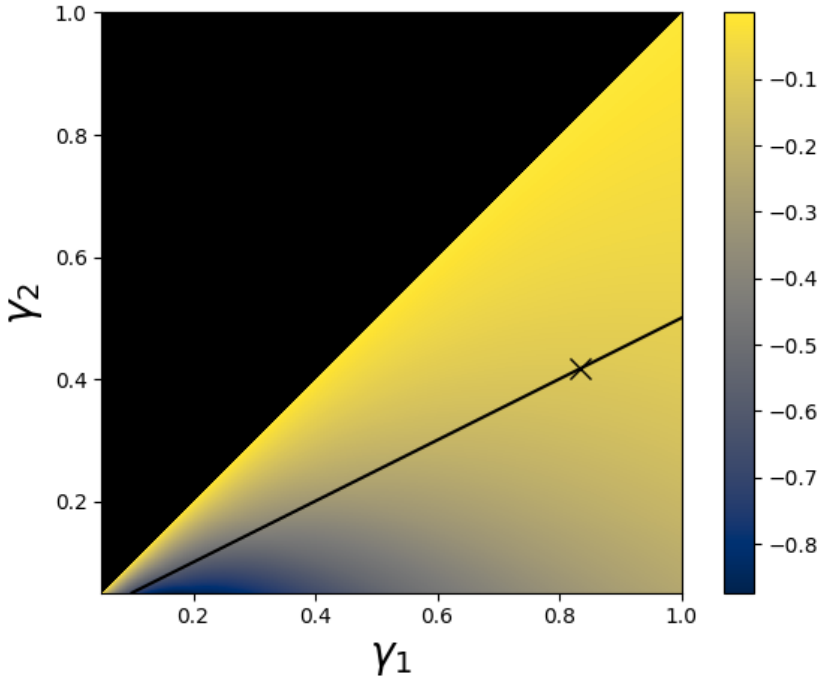

Figure S2: The values taken by w_{ℓ^*} as a function of γ_1 and γ_2, at $\sigma/R = 0.1$. The values taken by γ_1 γ_2 are chosen so that the range of the potential is always between the size of the particle (σ^*) and the diameter of the sphere $2R$. The black background corresponds to regions that have not been explored (where $\gamma_1 < \gamma_2$). The solid black line corresponds to $\gamma_1 = 2\gamma_2$, and the cross denotes the choice $\gamma_1 = \frac{5}{6}$ and $\gamma_2 = \frac{1}{2}\gamma_1$.

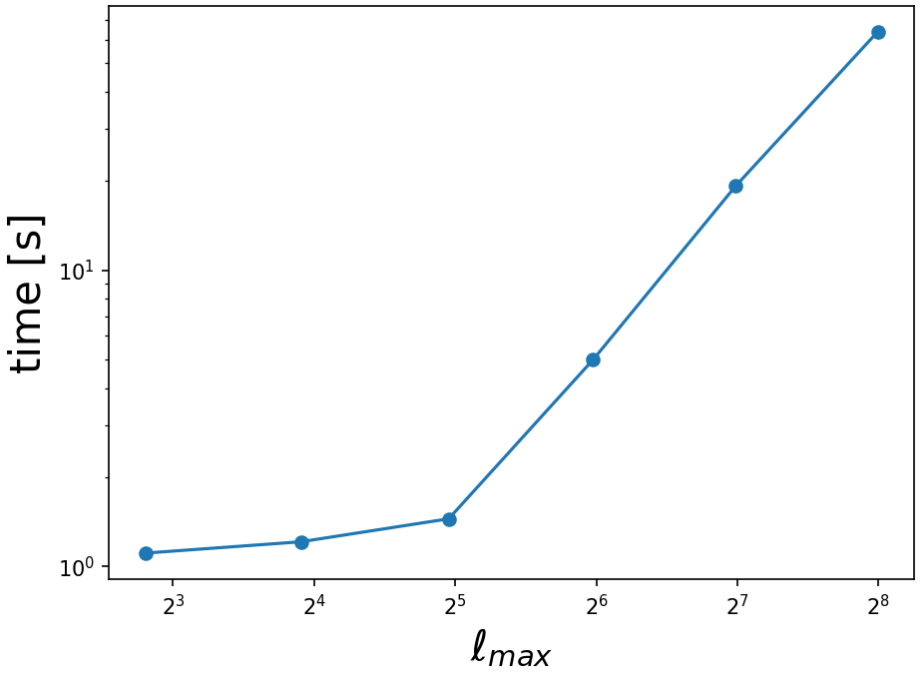

Figure S3: Median time for a grand potential minimization with different starting density profiles as the maximum harmonic degree ℓ_{max} increases. Because of the sampling theorem[Driscoll and Healy(1994)], the choice of ℓ_{max} determines the number of sampled grid points, as it fixes $K = 2(\ell_{max} + 1)$ (for a grid of $K \times 2K$ points). We used $\ell_{max} = 127$ to obtain our results in the main text, which corresponds to $K = 256$. This was chosen to limit the convergence time, which would increase by a factor ~ 10 for $\ell_{max} = 255$.

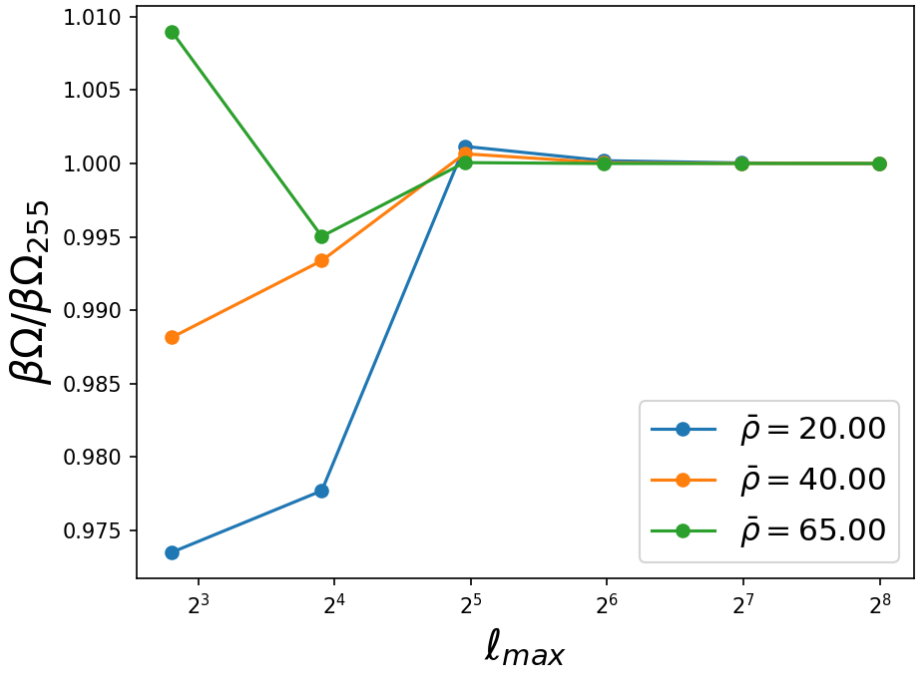

Figure S4: Convergence of the grand potential $\beta\Omega$ of the equilibrium distribution as ℓ_{max} is increased, for three different trial densities $\bar{\rho}$. All grand potentials are divided by the value $\beta\Omega$ takes at $\ell_{max} = 255$. As shown in the figure, even at the lowest value for ℓ_{max} there is only a $\sim 1\%$ variation between the values of $\beta\Omega$ at $\ell_{max} = 7$ and the ones computed for the highest sampled density profiles at $\ell_{max} = 255$. Moreover the convergence is very quick, as setting $\ell_{max} = 31$ is enough to reduce the discrepancy between computed grand potentials by another order of magnitude.

(a) $\ell_{max} = 7$

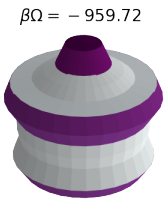

(b)

(c)

(d) $\ell_{max} = 15$

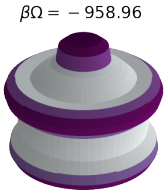

(e)

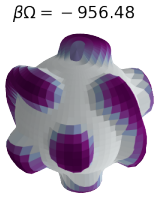

(f)

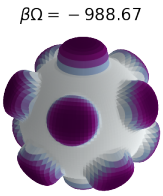

(g) $\ell_{max} = 31$

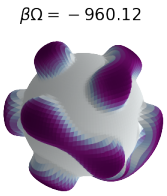

(h)

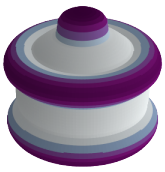

(i)

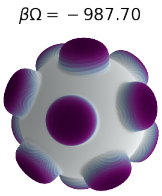

(j) $\ell_{max} = 63$

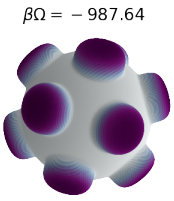

(k)

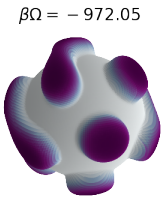

(l)

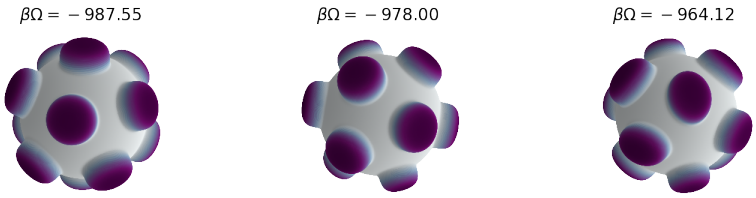

(m) $\ell_{max} = 127$ (n) (o)

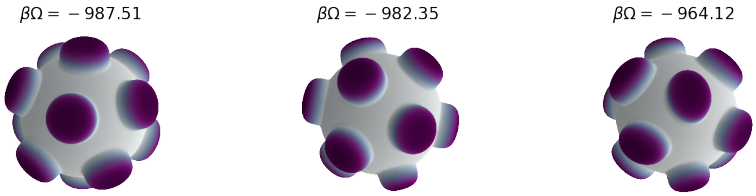

(p) $\ell_{max} = 255$ (q) (r)

Figure S5: Density profiles of the equilibrium distributions at $\bar{\rho} = 20$ as ℓ_{max} increases (first column), along with the second and third most stable distributions (second and third column respectively). Different distributions are obtained by starting the minimization from different density profiles. The 12-cluster crystal is always the equilibrium distribution, but the other distributions vary as ℓ_{max} increases. Interestingly, a different configuration with 12 clusters appears as the third most stable distribution at $\ell_{max} > 127$: in this case, 8 clusters have 4 neighbors and the others have 6. This build up of topological charges (since 4-fold disclinations hold twice the topological charge of 5-fold disclinations) seems to be connected to an increase in the grand potential $\beta\Omega$, which prevents this configuration from being the equilibrium one.

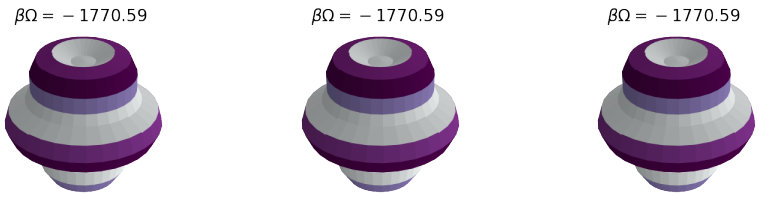

(a) $\ell_{max} = 7$ (b) (c)

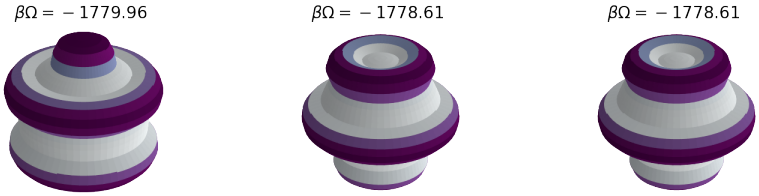

(d) $\ell_{max} = 15$ (e) (f)

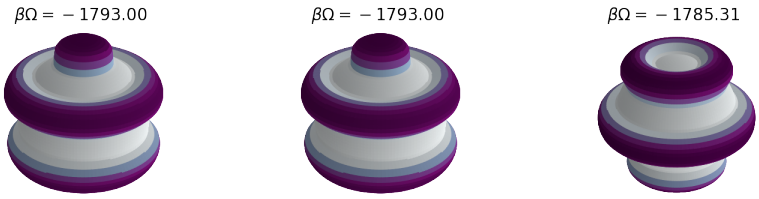

(g) $\ell_{max} = 31$ (h) (i)

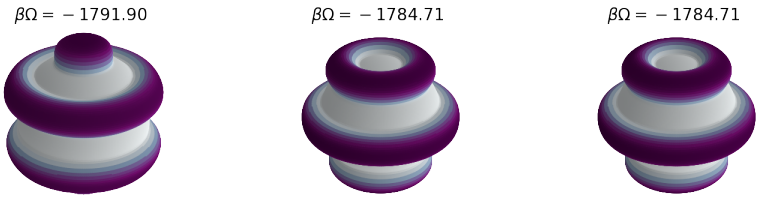

(j) $\ell_{max} = 63$ (k) (l)

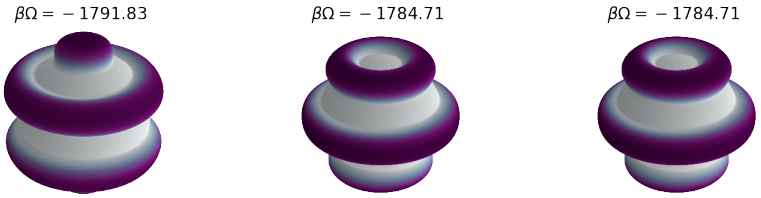

(m) $\ell_{max} = 127$ (n) (o)

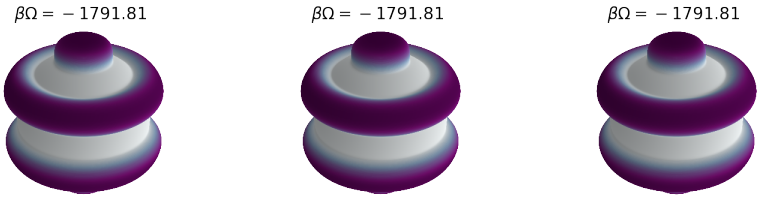

(p) $\ell_{max} = 255$ (q) (r)

Figure S6: Density profiles of the equilibrium distributions at $\bar{\rho} = 40$ as ℓ_{max} increases (first column), along with the second and third most stable distributions (second and third column respectively). Different distributions are obtained by starting the minimization from different density profiles. While the 4-stripe configuration is usually the equilibrium one, for $\ell_{max} = 7$ we do not encounter it.

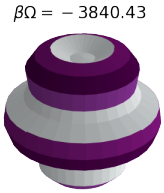

(a) $\ell_{max} = 7$

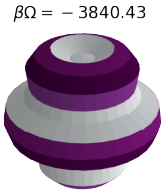

(b)

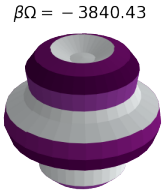

(c)

(d) $\ell_{max} = 15$

(e)

(f)

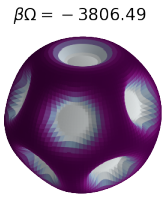

(g) $\ell_{max} = 31$

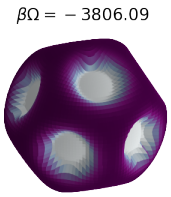

(h)

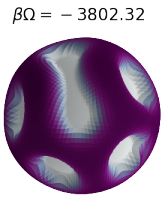

(i)

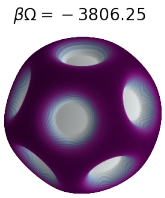

(j) $\ell_{max} = 63$

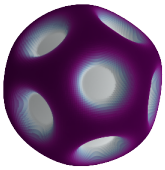

(k)

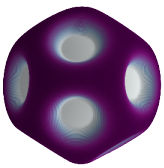

(l)

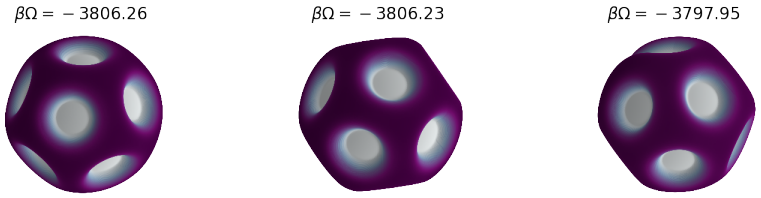

(m) $\ell_{max} = 127$ (n) (o)

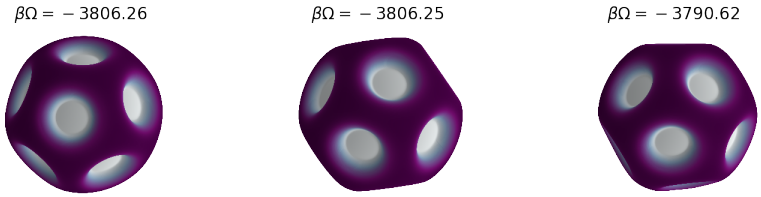

(p) $\ell_{max} = 255$ (q) (r)

Figure S7: Density profiles of the equilibrium distributions at $\bar{\rho} = 65$ as ℓ_{max} increases (first column), along with the second and third most stable distributions (second and third column respectively). Different distributions are obtained by starting the minimization from different density profiles. While the 12-bubble configuration is usually the equilibrium one, for $\ell_{max} = 7$ we do not encounter it.

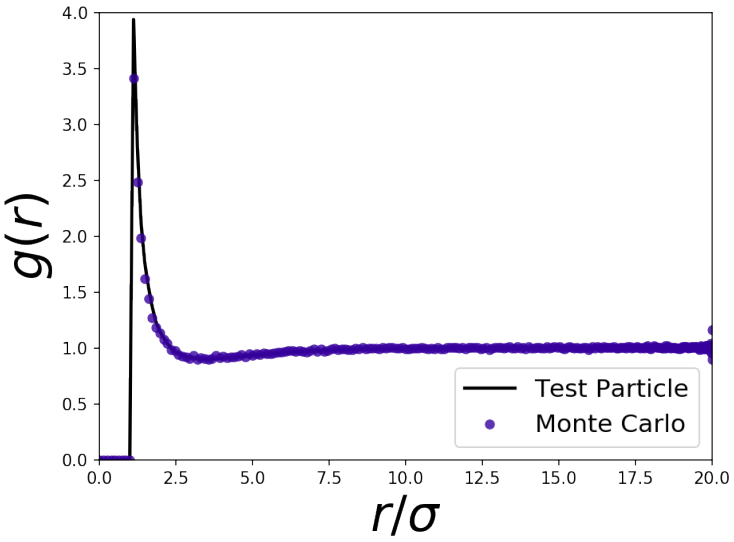

(a) $N = 10$, $\rho R^2 = 0.80$

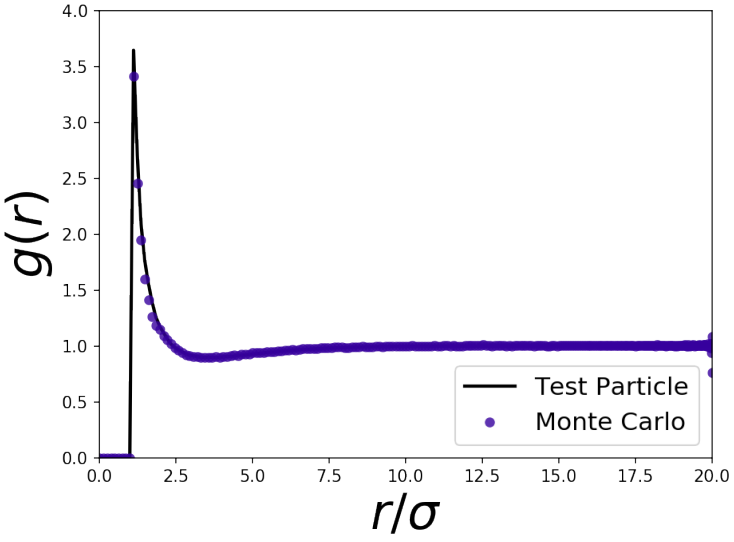

(b) $N = 25$, $\rho R^2 = 1.99$

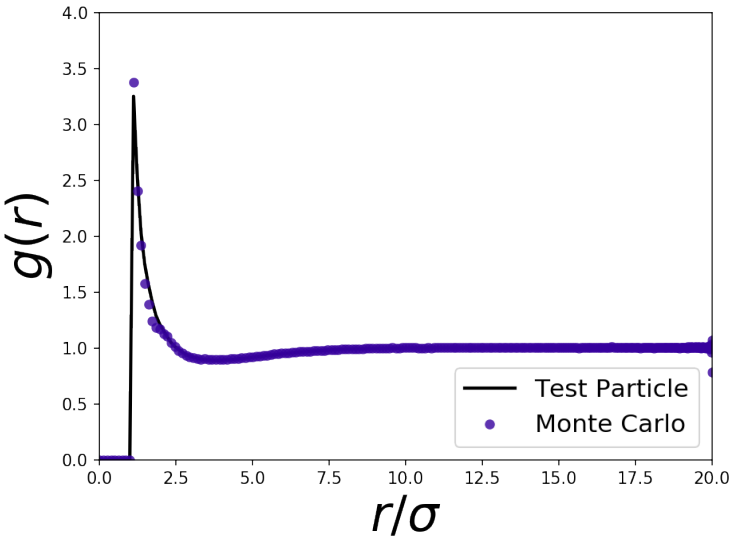

(c) $N = 50$, $\rho R^2 = 3.98$

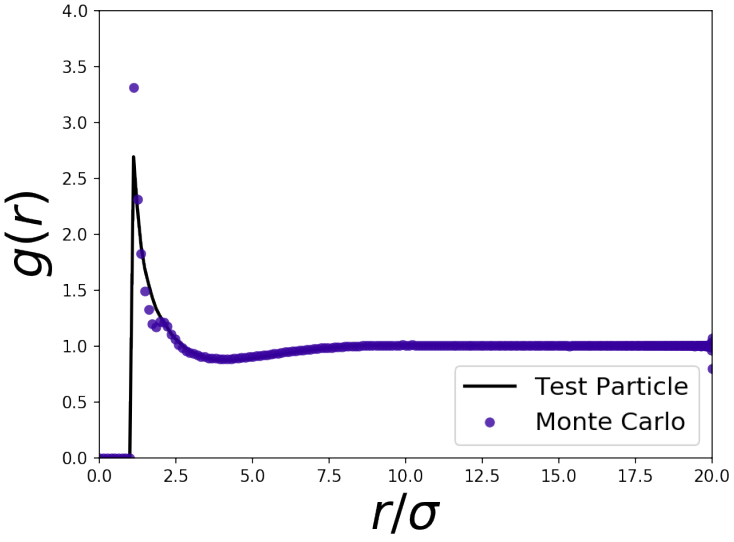

(d) $N = 100$, $\rho R^2 = 7.96$

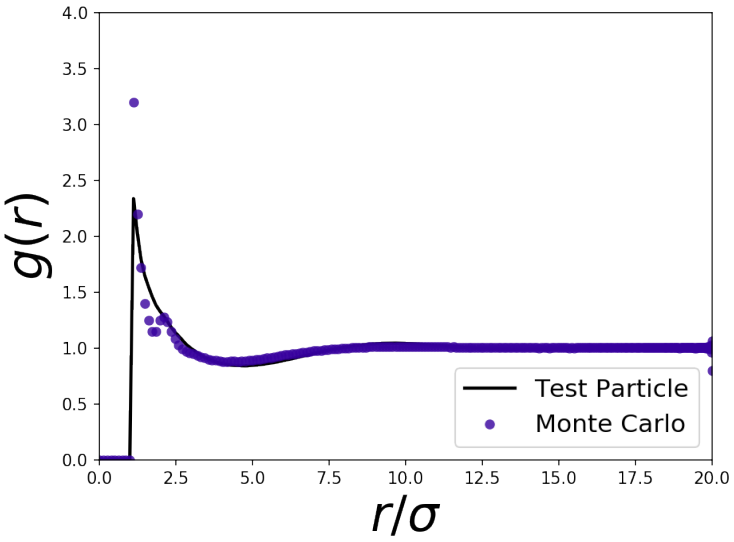

(e) $N = 150$, $\rho R^2 = 11.94$

Figure S8: Correlation functions computed at different densities and $\sigma/R = 0.1$, $T^* = 1.0$. The kink at $r/\sigma = 2.5$ only appears at large densities, hinting that its presence is linked to intra-cluster packing effects.